PERGAMON

International Journal of Solids and Structures 38 (2001) 1721–1735

INTERNATIONAL JOURNAL OF SOLIDS and STRUCTURES

www.elsevier.com/locate/ijsolstr

A micromechanically based couple–stress model of an elastic two-phase composite

Frederic Bouyge [a], Iwona Jasiuk [a], Martin Ostoja-Starzewski [b,*]

[a] *The George W. Woodruff School of Mechanical Engineering, Georgia Institute of Technology, Atlanta, GA 30332-0405, USA*
[b] *Institute of Paper Science and Technology, Engineering and Paper Materials Division, Georgia Institute of Technology, 500 10th Street, NW, Atlanta, GA 30318-5794, USA*

Received 22 September 1999; in revised form 13 February 2000

Abstract

The study reported in this paper concerns the determination of couple–stress moduli and characteristic lengths of heterogeneous materials. The study is set in the context of a planar (two-dimensional), two-phase composite with linear non-couple–stress (classical), elastic constituents, with a single microstructural length scale (inclusion spacing) in an equilateral triangular array. We use an approach which allows a replacement of this composite by an approximating couple–stress continuum. We determine the effective material parameters from the response of a unit cell under either displacement, displacement-periodic, or traction boundary conditions. We carry out computations of all the moduli by varying the stiffness ratio of both phases, so as to cover a range of very different materials from porous solids through composites with rigid inclusions. It is found that the three boundary conditions result in hierarchies of couple–stress moduli. In addition, we observe from our numerical computations that these three boundary conditions also result in a hierarchy of characteristic lengths.

Keywords: Elastic composite; Couple–stress model

1. Introduction

Classical continuum theories show discrepancies with experiments when a material microstructure gives rise to sharp gradients of dependent fields. Cosserat-type (or microcontinuum-type) theories, dating back to the Cosserat brothers (Cosserat, 1909), attempt to account for these phenomena. Although a number of theoretical results have been obtained, the full utility of Cosserat-type theories hinges on one's ability to determine the constitutive coefficients. Indeed, some progress in that direction has been made over the past three decades, but the situation is still one of theoreticians being well ahead of the experimentally available results (e.g., Nowacki, 1986a,b). The work we report here aims at remedying the situation through micromechanical analysis rather than the experiment.

* Corresponding author. Tel.: +1-404-894-6646; fax: +1-404-894-4778.
E-mail address: martin.ostoja@ipst.edu (M. Ostoja-Starzewski).

0020-7683/01/$ - see front matter
PII: S0020-7683(00)00132-3

It appears that, in general, the issue of determination of micropolar coefficients has been addressed in four types of problems: (a) crystal lattice systems (Askar, 1986); (b) regular beam networks (Woźniak, 1970; Bazant and Christensen, 1972); (c) laminated composites (Herrmann and Achenbach, 1968); and (d) granular media and foams (Perkins and Thomson, 1973; Lakes, 1983, 1986, 1995, and Yang and Lakes, 1982). All these systems have one feature in common: they exhibit some definite microstructure, which, as is well known, forms the motivation of all the investigations of Cosserat-type models and theories.

Thus, works in the first and second categories start out with a very clearly set periodic system of particles interacting via forces and moments modeled by either interatomic potentials or beams. Laminated composites offer quite a similar advantage thanks to their clearly defined geometry. The situation with foams and granular media is more difficult due to a spatially disordered geometry of those materials, and therefore, they have principally been studied through experiments.

In a recent study, Forest and Sab (1998) proposed a methodology for the derivation of an effective, homogeneous Cosserat-type continuum for a heterogeneous Cauchy-type continuum. Their approach is an extension of the classical homogenization method (Sanchez-Palencia and Zaoui, 1987) – it hinges on a representation of the macroscopic displacement field by a polynomial main field and a periodic perturbation. More specifically, they show three levels of the polynomial expansion: (i) the linear one leads to a classical Cauchy-type continuum, (ii) the quadratic one leads to a couple–stress continuum, also called a *restricted model* by Nowacki (1986a,b), and (iii) the third-order one (respectively, fourth order in three dimensions) leads to an unrestricted Cosserat-type (micropolar) continuum. Using a finite element method, Forest and Sab also demonstrate the definite advantage of replacing the actual Cauchy-type microstructure by the Cosserat-type continuum: a much smaller number of degrees of freedom is required in the homogenized model.

Model of type (ii) has recently been pursued by Ostoja-Starzewski et al. (1999). We carried out that study in the context of a planar, periodic, effectively isotropic, two-phase composite with linear elastic constituents of classical Cauchy type, with a microstructural length scale given by the inclusion spacing. We subjected the unit cell to periodic boundary conditions. In the limit of very low stiffness of the inclusion phase we have obtained moduli that showed very good agreement with analytical derivations of beam-framework models (Woźniak, 1970). Of additional interest to us was the determination of the somewhat enigmatic characteristic length l – a parameter apparently first introduced in the analytical studies in the sixties, when it showed up in the elastostatic field equations. While in the past, l was postulated to be equal to the average cell or grain size, with all the moduli in hand we could now easily compute l, and, in fact, found it to be a fraction of the microstructural cell size – from about one tenth to fourth of it – for composites of the type described at the beginning of this paragraph at volume fractions from 3.6–58%.

In this paper, we continue this initial study by considering couple–stress moduli and characteristic lengths of the above described composite under several additional types of boundary conditions: displacement, displacement-periodic, and traction boundary conditions. We then find that these boundary conditions result in hierarchies of couple–stress moduli. The motivation of this paper lies in the fact that we cannot apply periodic boundary conditions in one of the tests (the bending test). Thus, we use an alternate approach involving displacement and traction boundary conditions to obtain bounds on couple–stress moduli and compare those with periodic and displacement-periodic boundary condition results. This investigation complements our other studies of boundary condition effects on elastic moduli of composites, e.g. Jiang et al. (2000).

2. Problem formulation

The leitmotif of this paper is to replace a complex microstructure by a higher-order (i.e., Cosserat) continuum. Once done, this allows one to work with a homogeneous material model, endowed with yet an

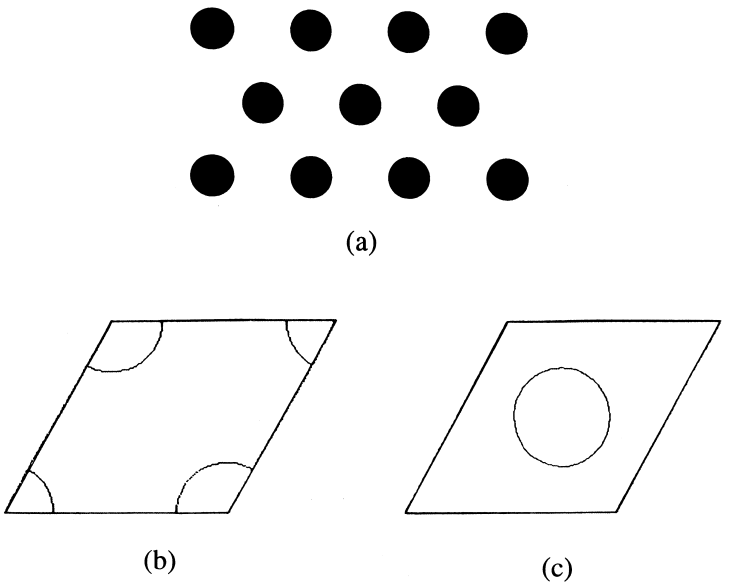

Fig. 1. (a) A periodic, globally isotropic, matrix-inclusion composite, of period L, with inclusions of diameter d; (b) a periodic unit cell with inclusions at the corner; and (c) a periodic unit cell with an inclusion at the center.

extra degree of freedom – that of rotation. In this paper, we address the issue of effective couple–stress moduli in the context of linear elastic microstructures with a single microstructural length scale such as the mean inclusion spacing. In particular, we remove the aspect of geometric disorder by focusing on a periodic composite material with an equilateral, triangular arrangement of circular inclusions. This geometry gives us a composite material which is effectively isotropic. We take the periodic unit cell as a rhombus-shaped domain of edge length L and volume $V = bL^2\sqrt{3}/2$ (Fig. 1). The rhombus' height in the x_2 direction is $H = 2h = L\sqrt{3}/2$, and its thickness in the x_3 is b.

The inclusion (i) and matrix (m) phases follow classical (linear elastic, isotropic) elasticity; they have Young's moduli E^{i} and E^{m}, and Poisson's ratios ν^{i} and ν^{m}, respectively. By varying the stiffness ratio $E^{\mathrm{i}}/E^{\mathrm{m}}$ we can model a wide range of materials with either stiff or soft inclusions, and in the extreme cases of this ratio tending to either ∞ or 0, we approach composites with rigid inclusions or pores. It is important to note, however, that the special case of no mismatch ($E^{\mathrm{i}}/E^{\mathrm{m}} = 1$) implies no microstructure, so the couple stress model becomes unnecessary in that case.

We focus here on the first planar problem of Cosserat elasticity (Nowacki, 1986a,b) with displacement $\boldsymbol{u} = (u_1, u_2, 0)$ and rotation $\boldsymbol{\varphi} = (0, 0, \varphi_3)$; this is a generalization of the classical in-plane elasticity, and consider a couple–stress (or, restricted continuum) model, in which rotation depends on displacement gradients in the same manner as in classical elasticity. The kinematics of the body is described by u_1, u_2, and $\varphi_3 = (u_{2,1} - u_{1,2})/2$, which define the strain tensor γ_{ij} and the (bending) curvature tensor $\kappa_{i3}, i, j = 1, 2$. The force field is specified by force-stress tensor τ_{ij} and couple–stress tensor $\mu_{i3}, i, j = 1, 2$.

The composite of Fig. 1 is centrosymmetric: there is no coupling between τ_{ij} and κ_{i3} on the one hand and between γ_{ij} and μ_{i3} on the other. Thus, the constitutive law will involve two stiffness tensors $C^{(1)}_{ijkl}$ and $C^{(2)}_{i3k3}$ only, which are defined via

$$\tau_{ij} = C^{(1)}_{ijkl}\gamma_{kl}, \quad \mu_{i3} = C^{(2)}_{i3k3}\kappa_{k3}, \qquad i, j, k, l = 1, 2. \tag{1}$$

Equivalently, we can work with their inverses: compliances $S^{(1)}_{ijkl}$ and $S^{(2)}_{i3k3}$. In the isotropic case, the latter is

$$S^{(1)}_{ijkl} = \tfrac{1}{4}[S(\delta_{ik}\delta_{jl} + \delta_{il}\delta_{jk}) + (A - S)\delta_{ij}\delta_{kl}], \quad S^{(2)}_{i3k3} = \delta_{ik}M, \tag{2}$$

where A, M and S are three independent planar couple–stress constants defined in Ostoja-Starzewski and Jasiuk (1995).

Note that A and S are the area bulk compliance and shear compliance, respectively, and they are the same as in classical plane elasticity. M is the additional independent constant, which has a dimension differing from A and S by length squared. This gives rise to a length scale present in the couple–stress theory (a special case of the Cosserat theory), which is absent in the classical elasticity theory. This length is quantitatively grasped by a characteristic length l defined as

$$l = \sqrt{\frac{S}{4M}} = \sqrt{\frac{S^{(1)}_{1212}}{S^{(2)}_{1313}}}. \tag{3}$$

In this paper, we obtain the effective response of composites by employing the couple–stress theory, which therefore gives the second constitutive tensor $C^{(2)}_{i3k3}$ (in addition to $C^{(1)}_{ijkl}$ present in classical theory), which captures the information on the microstructure. This information is not captured by classical micromechanics approaches for predictions of effective elastic moduli of heterogeneous materials.

Note that the unit cell's response under non-periodic boundary conditions is anisotropic, but the departure from isotropy is on the order of only a few percent for the composite systems with inclusion volume fraction of 18% studied in this paper. This makes an approximate comparison of stiffness tensors (both $C^{(1)}_{ijkl}$ and $C^{(2)}_{i3k3}$) found from non-periodic boundary conditions (this paper) with those from periodic ones (previous paper) possible. Additionally, this allows a discussion of all the results in the context of an isotropic material model.

3. Boundary conditions on the unit cell

The main goal of our analysis is the determination of effective constitutive coefficients from the unit cell response of a two-phase composite described in Section 2. We consider three types of boundary conditions for determination of the effective couple–stress moduli for a material domain B having boundary ∂B (Fig.1): (i) displacement, (ii) displacement-periodic, and (iii) traction controlled. In each case we compute, by a finite element method, the total elastic strain energy stored in the unit cell of the two-phase composite $U^{\text{cell}}(= U^{*\text{cell}})$ as a functional of Cauchy strains ε_{ij} (respectively, Cauchy stresses σ_{ij}). Separately, for the first two boundary conditions, we set up the energy $U^{\text{couple-stress}}$ corresponding to an effective, homogeneous couple–stress continuum, which is a functional of the strains γ_{ij} and the curvatures κ_{i3}. By setting

$$U^{\text{couple-stress}} = U^{\text{cell}}, \tag{4a}$$

we infer the effective stiffness tensors $C^{(1)}_{ijkl}$ and $C^{(2)}_{i3k3}$. On the other hand, in the case of traction boundary conditions, we work with the complementary energy $U^{*\text{couple-stress}}$ – a functional of τ_{ij} and μ_{i3} – and, from

$$U^{*\text{couple-stress}} = U^{*\text{cell}}, \tag{4b}$$

we obtain the effective compliance tensors $S^{(1)}_{ijkl}$ and $S^{(2)}_{i3k3}$.

3.1. Displacement boundary conditions

The total elastic strain energy stored in the unit cell is

$$U^{\text{cell}} = \frac{1}{2}\int_V \varepsilon_{ij} C_{ijkl} \varepsilon_{kl}\, \mathrm{d}V, \tag{5}$$

while that of an approximating couple–stress continuum involves, in general, two terms

$$U^{\text{couple-stress}} = \frac{V}{2}\left[\gamma_{ij}C^{(1)}_{ijkl}\gamma_{kl} + \kappa_{i3}C^{(2)}_{i3k3}\kappa_{k3}\right], \tag{6}$$

where γ_{ij} in Eq. (6) stands for the effective strain of the unit cell in the couple–stress continuum and κ_{i3} is the effective curvature; V is the volume of the unit cell B defined in Section 2.

To determine $C^{(1)}_{ijkl}$ we conduct two tests:

(i) *Uniaxial extension*

If we apply γ_{22}, the displacement boundary conditions become

$$u_1(\boldsymbol{x}) = 0, \quad u_2(\boldsymbol{x}) = \gamma_{22}x_2 \qquad \forall \boldsymbol{x} \in \partial B, \tag{7}$$

which yields $C^{(1)}_{2222} = 2U^{\text{cell}}/V$ when we set $\gamma_{22} = 1$; alternately, we could apply $u_1(\boldsymbol{x}) = \gamma_{11}x_1$ and $u_2(\boldsymbol{x}) = 0$, which would yield $C^{(1)}_{1111}$. For our composite, $C^{(1)}_{1111}$ is approximately (within 5%) equal to $C^{(1)}_{2222}$ for all the stiffness mismatches considered.

(ii) *Simple shear*

$$u_1(\boldsymbol{x}) = \gamma_{12}x_2, \quad u_2(\boldsymbol{x}) = 0, \quad \forall \boldsymbol{x} \in \partial B, \tag{8}$$

which yields $C^{(1)}_{1212} = 2U^{\text{cell}}/V$ when we set $\gamma_{12} = 1$. There are two more possibilities here: either apply $u_1(\boldsymbol{x}) = 0$ and $u_2(\boldsymbol{x}) = \gamma_{12}x_1$, or $u_1(\boldsymbol{x}) = \gamma_{12}x_2/2$ and $u_2(\boldsymbol{x}) = \gamma_{12}x_1/2$.

Finally, to determine $C^{(2)}_{i3k3}$, we conduct

(iii) *Bending test*

$$u_1(\boldsymbol{x}) = -x_1x_2\kappa_{13}, \quad u_2(\boldsymbol{x}) = \frac{x_1^2}{2}\kappa_{13} \quad \forall \boldsymbol{x} \in \partial B. \tag{9}$$

We note that, for a bending test, γ_{ij} in Eq. (6) may be zero or non-zero, depending on the coordinate system chosen. For the above bending test, the only possible non-zero strain component is $\gamma_{11} = \int_V u_{1,1}\,\mathrm{d}V/V = \int_{\partial B} u_1 n_1\,\mathrm{d}S/V$. When we take the origin of coordinates at the rhombus corner, Eq. (9) yields the average strain in the couple–stress medium $\gamma_{11} = -h\kappa_{13}$, which results in $C^{(2)}_{1313} = 2U^{\text{cell}}/V - h^2C^{(1)}_{1111}$, whereby (recall Eq. (4a)) $U^{\text{cell}} = U^{\text{couple-stress}} = V[\gamma_{11}C^{(1)}_{1111}\gamma_{11} + \kappa_{13}C^{(2)}_{1313}\kappa_{13}]/2$. When the origin of the coordinate system is at the cell's center, then $\gamma_{11} = 0$, and thus the term involving $C^{(1)}_{1111}$ in the latter expression vanishes. Also, here, there exists another possibility for carrying the bending test: $u_1(\boldsymbol{x}) = x_2^2\kappa_{23}/2$ and $u_2(\boldsymbol{x}) = -x_1x_2\kappa_{23}$. This test would yield $C^{(2)}_{2323}$, which, for our study, is only approximately equal to $C^{(2)}_{1313}$, given the anisotropy issue mentioned earlier.

The deformation modes for the above three tests under displacement boundary conditions are shown in Fig. 2. Note that in the last test (bending test) the coordinate system's origin is chosen at the lower left corner.

3.2. Displacement-periodic conditions

The energies U^{cell} and $U^{\text{couple–stress}}$ are given by Eqs. (5) and (6), respectively. Here we choose to apply the displacement boundary conditions on the two horizontal boundaries of the rhombus ∂B_{d}, and the periodic boundary conditions on the remaining slanted boundaries $\partial B_{\text{p}} = \partial B - \partial B_{\text{d}}$.

To determine $C^{(1)}_{ijkl}$ we conduct two tests:

(i) *Uniaxial extension*: If we apply γ_{22}, the periodic boundary conditions are given by

$$u_i(\boldsymbol{x} + L\boldsymbol{e}_1) = u_i(\boldsymbol{x}), \quad t_i(\boldsymbol{x} + L\boldsymbol{e}_1) = -t_i(\boldsymbol{x}) \qquad \forall \mathbf{x} \in \partial B_{\text{p}}, \tag{10}$$

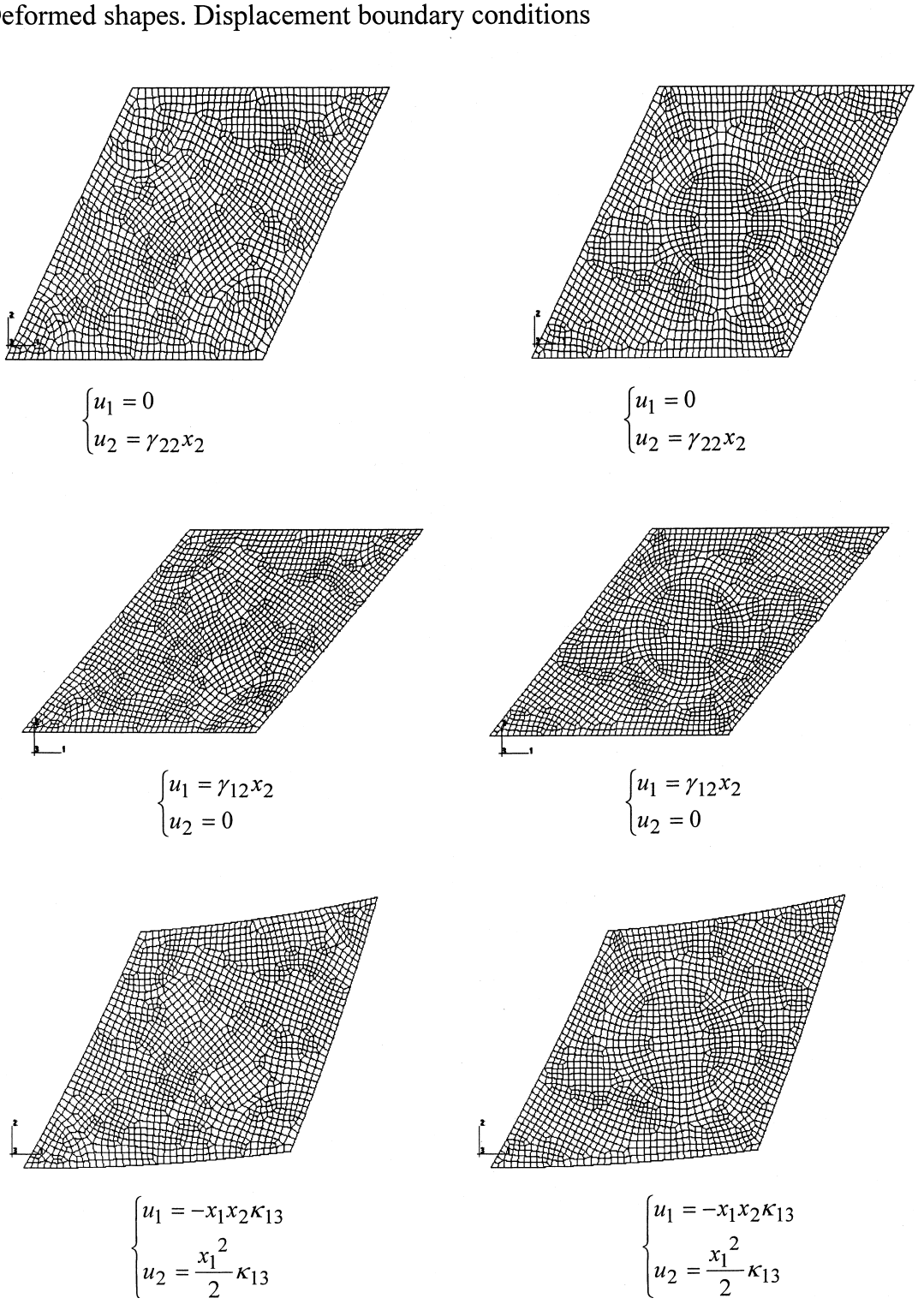

Fig. 2. Tests for the determination of couple–stress constants $C^{(1)}_{2222}$, $C^{(1)}_{1212}$, and $C^{(2)}_{1313}$ under displacement boundary conditions. Left (right) column corresponds to the inclusion at the corner (center).

and the displacement boundary conditions are given by Eq. (7) on ∂B_d; $\boldsymbol{e}_1$ is the unit vector along x_1. Thus, the controlled uniaxial extension $\gamma_{22} = 1$ yields $C^{(1)}_{2222} = 2U^{\text{cell}}/V$. Of course, alternately, we could apply γ_{11} so that the periodic boundary conditions on slanted faces would take the form $u_i(\boldsymbol{x} + L\boldsymbol{e}_1) = u_i(\boldsymbol{x}) + \gamma_{11}L\boldsymbol{e}_1$ and $t_i(\boldsymbol{x} + L\boldsymbol{e}_1) = -t_i(\boldsymbol{x})$, while the displacement boundary conditions on horizontal faces would be $u_1(\boldsymbol{x}) = \gamma_{11}x_1$ and $u_2(\boldsymbol{x}) = 0$.

(ii) *Simple shear*: The periodic boundary conditions are given by

$$u_i(\boldsymbol{x} + L\boldsymbol{e}_1) = u_i(\boldsymbol{x}), \qquad t_i(\boldsymbol{x} + L\boldsymbol{e}_1) = -t_i(\boldsymbol{x}), \qquad \forall \boldsymbol{x} \in \partial B_p \tag{11}$$

and the displacement boundary conditions by

$$u_1(\boldsymbol{x}) = \gamma_{12}x_2, \quad u_2(\boldsymbol{x}) = 0 \quad \forall \boldsymbol{x} \in \partial B_d. \tag{12}$$

This yields $C^{(1)}_{1212} = 2U^{\text{cell}}/V$ (when we set $\gamma_{12} = 1$).

To determine $C^{(2)}_{i3k3}$, we conduct:

(iii) *Bending test*:

The periodic boundary conditions are given by

$$\begin{aligned} u_1(\boldsymbol{x} + L\boldsymbol{e}_1) &= u_1(\boldsymbol{x}) - x_1x_2\kappa_{13}\big|_{\partial B_p} \\ u_2(\boldsymbol{x} + L\boldsymbol{e}_1) &= u_2(\boldsymbol{x}) + \frac{x_1^2}{2}\kappa_{13}\bigg|_{\partial B_p} \qquad \forall \boldsymbol{x} \in \partial B_p, \\ t_i(\boldsymbol{x} + L\boldsymbol{e}_1) &= -t_i(\boldsymbol{x}) \end{aligned} \tag{13}$$

while the displacement conditions on $\partial B_d = \partial B - \partial B_p$ are given by Eq. (9). Again, noting that $\gamma_{11} = \int_V u_{1,1}\,\mathrm{d}V/V = \int_{\partial B} u_1 n_1 \mathrm{d}S/V = -h\kappa_{13}$, if we take the origin of the coordinate system at the corner, this yields $C^{(2)}_{1313} = 2U^{\text{cell}}/V - h^2C^{(1)}_{1111}$ in the same fashion as before.

The deformation modes for the above three tests under displacement-periodic boundary conditions are shown in Fig. 3, with the origin of the coordinate system being chosen at the rhombus' left corner.

In Ostoja-Starzewski et al. (1999), we computed the $C^{(1)}_{ijkl}$ tensor under purely periodic boundary conditions, but the $C^{(2)}_{i3k3}$ tensor under displacement-periodic boundary conditions. The use of periodic boundary conditions applied to all surfaces for the evaluation of $C^{(1)}_{ijkl}$ is natural for a periodic microstructure considered and gives exact effective moduli. However, the test for the evaluation of $C^{(2)}_{i3k3}$, which involves bending, does not give a deformation which is periodic on horizontal faces of a rhombus-shaped unit cell. Thus, we could not use periodic boundary conditions on all surfaces, and have used displacement-periodic boundary conditions for bending test instead. For consistency, in the present computation we use the same boundary conditions (displacement-periodic) for both $C^{(1)}_{ijkl}$ and $C^{(2)}_{i3k3}$. In addition, we use displacement (as described already) and traction conditions which bound periodic and displacement-periodic results.

3.3. Traction conditions

The total complementary energy stored in the unit cell is

$$U^{*\text{cell}} = \frac{1}{2}\int_V \sigma_{ij}S_{ijmn}\sigma_{mn}\,\mathrm{d}V, \tag{14}$$

while that of an approximating couple–stress continuum involves, in general, two terms

$$U^{*\text{couple-stress}} = \frac{V}{2}\left[\tau_{ij}S^{(1)}_{ijmn}\tau_{mn} + \mu_{i3}S^{(2)}_{i3k3}\mu_{k3}\right]. \tag{15}$$

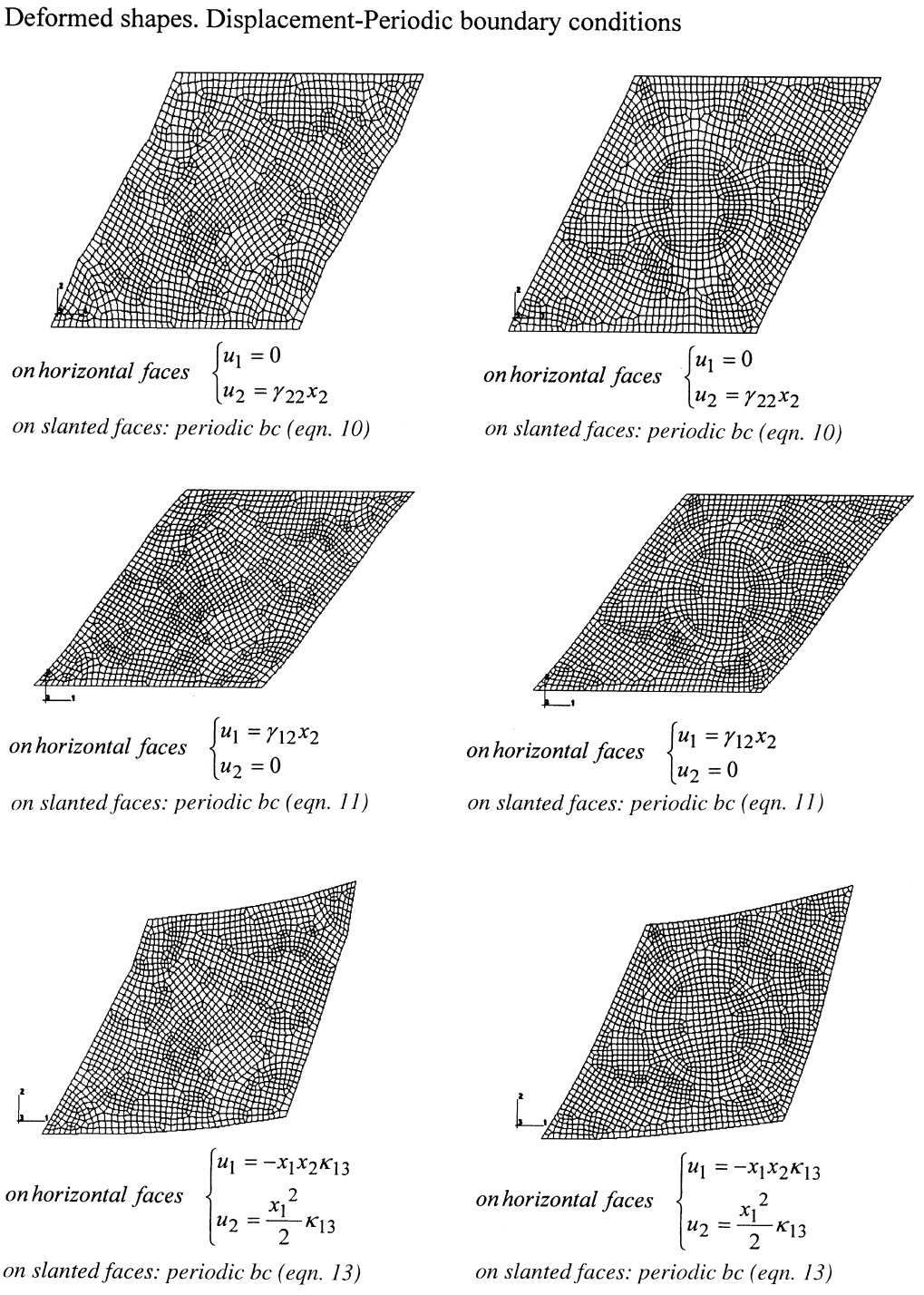

Fig. 3. Tests for the determination of constants $C^{(1)}_{2222}$, $C^{(1)}_{1212}$, and $C^{(2)}_{1313}$ under displacement–periodic boundary conditions given by Eqs. (10), (11) and (13). Left (right) column corresponds to the inclusion at the corner (center).

To determine $S^{(1)}_{ijkl}$ we conduct two tests:

(i) *Uniaxial tension*

$$t_1(\boldsymbol{x}) = \tau_{11} n_1, \quad t_2(\boldsymbol{x}) = 0 \quad \forall \boldsymbol{x} \in \partial B, \tag{16}$$

which yields $S^{(1)}_{1111} = 2U^{*\text{cell}}/V$ (when we set $\tau_{11} = 1$). Application of the τ_{22} loading (to get $S^{(1)}_{2222}$) is unwieldy because of the unbalanced moment imposed by this loading.

(ii) *Simple shear traction*

$$t_1(\boldsymbol{x}) = \tau_{12} n_2, \quad t_2(\boldsymbol{x}) = \tau_{12} n_1 \qquad \forall \boldsymbol{x} \in \partial B, \tag{17}$$

which yields $S^{(1)}_{1212} = 2U^{*\text{cell}}/V$ (when we set $\tau_{12} = 1$).

Finally, we conduct

(iii) *Bending test*

$$t_1(\boldsymbol{x}) = \sigma_{11} n_1 = c x_2 n_1, \quad t_2(\boldsymbol{x}) = 0 \qquad \forall \boldsymbol{x} \in \partial B, \tag{18}$$

where $c = M_{\text{B}}/I$ (M_{B} being the bending moment and $I = 2bh^3/3$ the moment of inertia); Eq. (18) yields $S^{(2)}_{1313}$. In this computation, we assumed the origin of the coordinate system at the cell's center, so that $S^{(2)}_{1313} = 2U^{*\text{cell}}/V$, whereby $U^{*\text{cell}} = U^{*\text{couple-stress}} = V\mu_{13}S^{(2)}_{1313}\mu_{13}/2$ with $\mu_{13} = M_{\text{B}}/area$ ($area = Lb\sqrt{3}/2$). Note that, in this case, the average couple–stress in the couple–stress medium $\tau_{11} = 0$. However, for other choices of coordinate system's origin, $\tau_{11} = \frac{1}{V}\int_V \sigma_{11}\,\mathrm{d}V = \frac{1}{V}\int_{\partial B} \sigma_{11} n_1 x_1\,\mathrm{d}S$ will, in general, not vanish.

Deformation modes for these tests under traction boundary conditions are shown in Fig. 4. As mentioned above, in the bending test under traction boundary conditions, the coordinate system is chosen at the center of a unit cell.

4. Couple–stress moduli: results and discussion

As pointed out in Section 2, by varying the stiffness ratio $E^{\text{i}}/E^{\text{m}}$ we can model a very wide spectrum of composite materials with either stiff or soft inclusions. Moreover, in the extreme cases of this ratio tending to very high or low numbers, we approach composites with rigid inclusions or pores, respectively; the actual values of ∞ or 0 cannot be set in our computational mechanics model. In the latter case, by raising the volume fraction of inclusions, we could arrive at the situation of cellular solids, which are essentially beam-network systems, Fig. 1(b). On the other hand, the case of inclusions of finite stiffness in a near-zero stiffness matrix would approach the setting of granular media, Fig 1(c).

The choice of unit cells required to determine the couple–stress moduli is as follows: (i) for beam networks and systems with soft inclusions, the cell is centered at the beam connection nodes; (ii) for granular-type media, with soft matrix material, the unit cell is centered at the grain center. This leads to a rule of placement of unit cells in two-phase composite materials: *the unit cell should be centered in a stiffer phase*. As the stiffness ratio of two phases tends to 1, the unit cell's placement has an ever smaller effect, until in the physically singular case of no mismatch, it becomes immaterial. This special case is of no interest to us as here the material is homogeneous with no microstructure, and thus, is described by the classical elasticity theory. Summarizing, when the contrast is 1 – i.e., when both phases are identical – one should use an RVE at the scale much smaller than what we show in our Figs. 1–4. This new scale should be defined by the presence of another microscale – crystal lattice or molecular, – and may also be Cosserat-type (e.g., Askar, 1986).

The complete computational mechanics procedure runs as follows:

1. For a given type of boundary conditions, the rhombus-shaped periodic unit cells of Fig. 1(b) and (c) are analyzed using the finite element software ABAQUS (1995), see Figs. 2–4.

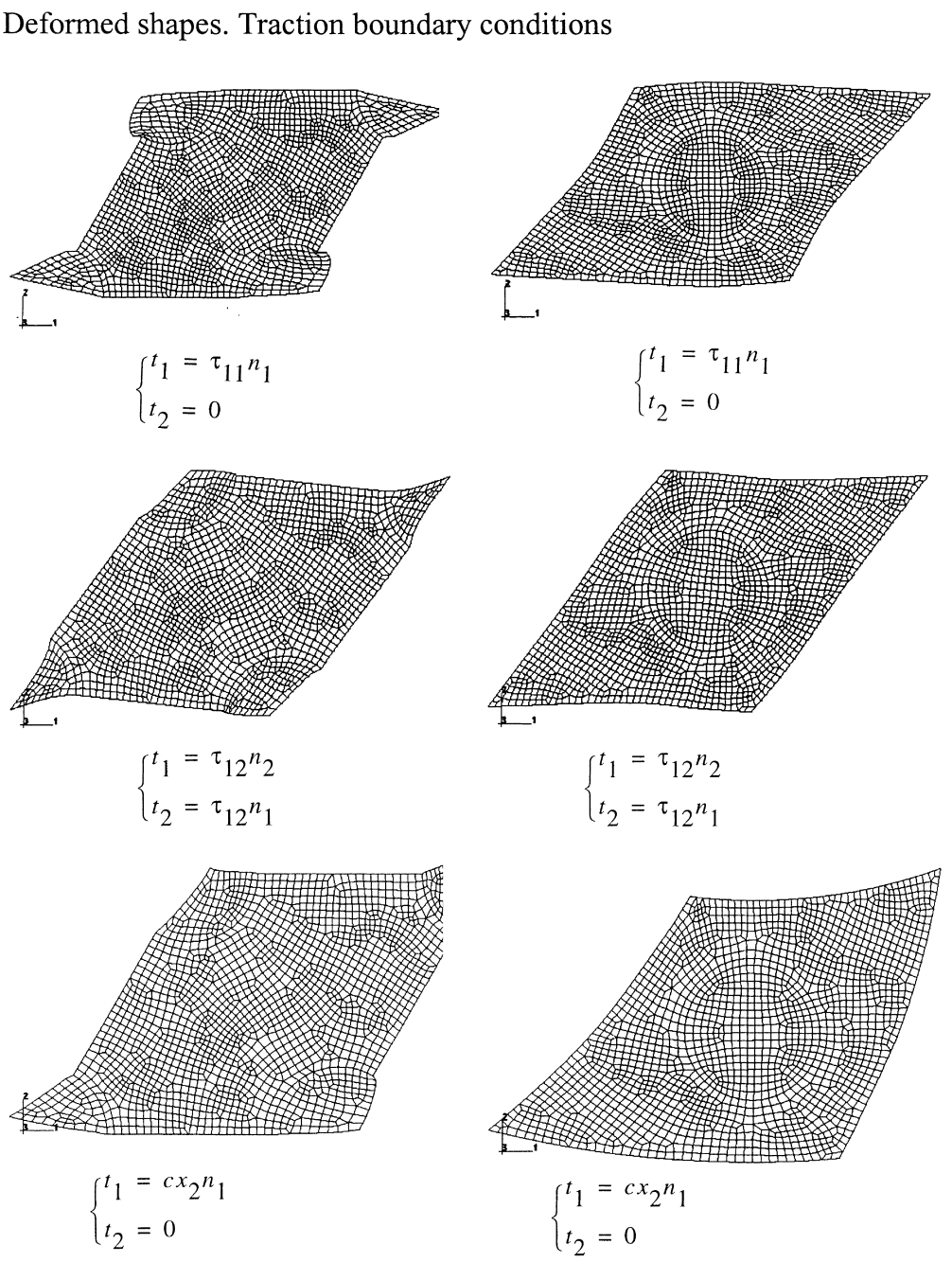

Fig. 4. Tests for the determination of constants $S^{(1)}_{1111}$, $S^{(1)}_{1212}$, and $S^{(2)}_{1313}$ under traction boundary conditions. Left (right) column corresponds to the inclusion at the corner (center).

2. Note that the equality $C^{(1)}_{1122} = C^{(1)}_{1111} - 2C^{(1)}_{1212}$, valid for isotropic media, which is only approximately satisfied for our case (within 3%), yields $C^{(1)}_{1122}$ directly. The same holds for compliances in case of the traction boundary condition.

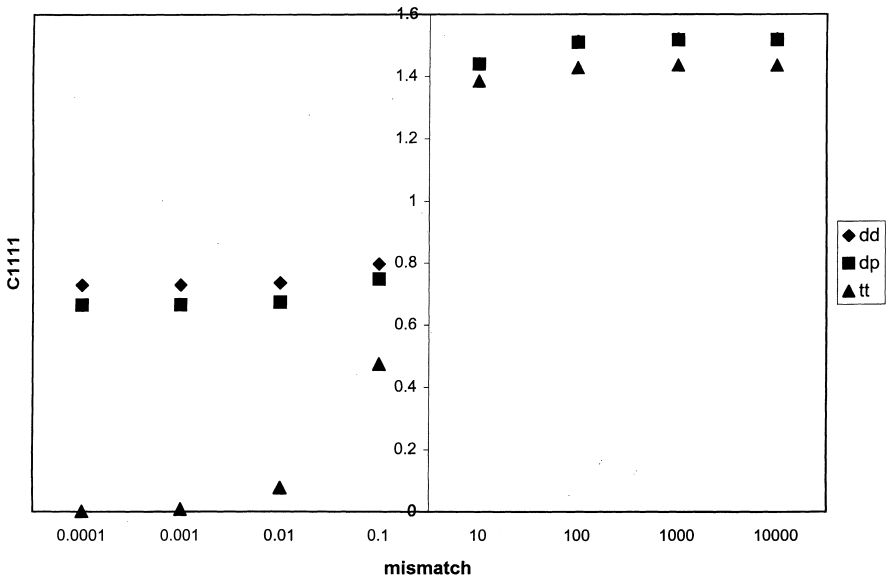

Fig. 5. The effective moduli $C^{(1)}_{1111} \cong C^{(1)}_{2222}$, non-dimensionalized by E^{m}, from three types of boundary conditions (displacement (dd), displacement-periodic (dp), and traction (tt)) plotted as functions of the stiffness ratio $E^{\mathrm{i}}/E^{\mathrm{m}}$ (mismatch) for the case of the Poisson's ratio $\nu^{\mathrm{m}} = \nu^{\mathrm{i}} = 0.3$ at volume fraction 18.4%.

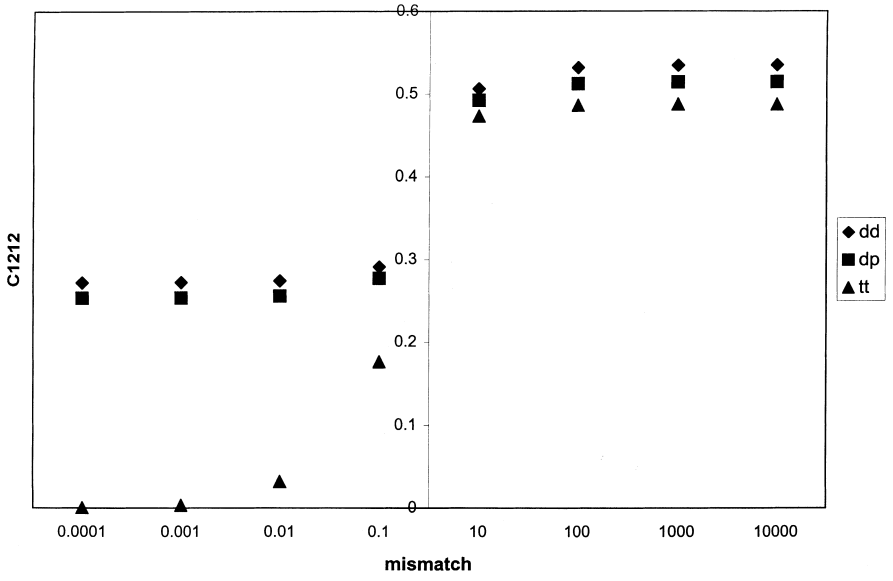

Fig. 6. The effective moduli $C^{(1)}_{1212}$, non-dimensionalized by E^{m}, from three types of boundary conditions plotted as functions of the stiffness ratio $E^{\mathrm{i}}/E^{\mathrm{m}}$ (mismatch) for the case of Poisson's ratio $\nu^{\mathrm{m}} = \nu^{\mathrm{i}} = 0.3$ at volume fraction 18.4%.

3. If the displacement or displacement-periodic conditions are being employed, compute, by inversion, the compliance components $S^{(1)}_{1111}, S^{(1)}_{1212}$, and $S^{(2)}_{1313}$.
4. Compute l from Eq. (3).

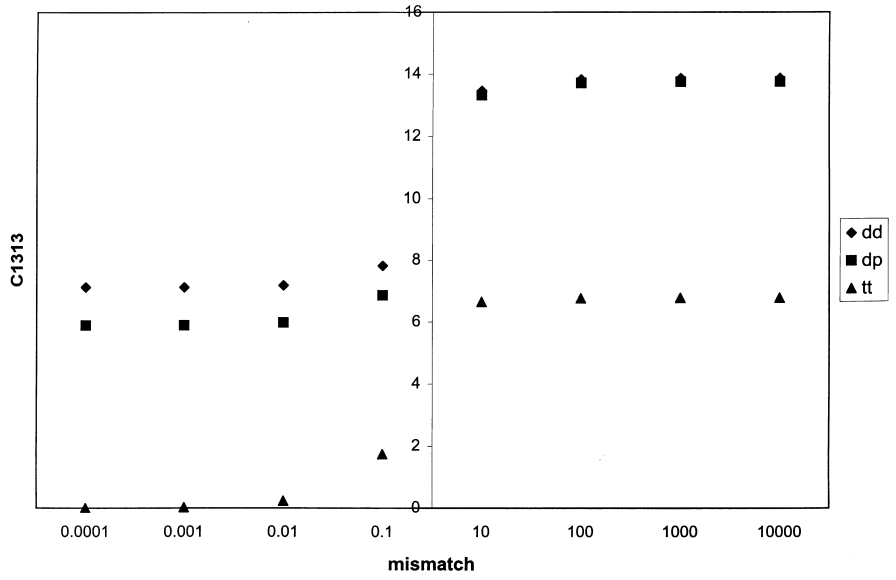

Fig. 7. The effective moduli $C^{(2)}_{1313}$, non-dimensionalized by E^{m}, from three types of boundary conditions plotted as functions of the stiffness ratio $E^{\mathrm{i}}/E^{\mathrm{m}}$ (mismatch) for the case of Poisson's ratio $v^{\mathrm{m}} = v^{\mathrm{i}} = 0.3$ at volume fraction 18.4%.

In Figs. 5–7, we present $C^{(1)}_{1111} \cong C^{(1)}_{2222}, C^{(1)}_{1212}$, and $C^{(2)}_{1313}$, respectively, obtained from each of three boundary conditions. They are plotted as functions of the stiffness ratio $E^{\mathrm{i}}/E^{\mathrm{m}}$, ranging from 10^{-4} to 10^{4} for the matrix Poisson's ratio $v^{\mathrm{m}} = 0.3$ and the inclusion Poisson's ratio $v^{\mathrm{i}} = 0.3$, and are non-dimensionalized by E^{m}. Note that the results of displacement-periodic boundary conditions always fall between those obtained by applying displacement and traction boundary conditions. Given the fact that γ_{ij} is symmetric, we can readily adapt the order relations formulated for apparent response tensors in classical elasticity (Hazanov and Huet, 1994)

$$\gamma_{ij}C^{(1)(tt)}_{ijkl}\gamma_{kl} \leqslant \gamma_{ij}C^{(1)(dp)}_{ijkl}\gamma_{kl} \leqslant \gamma_{ij}C^{(1)(dd)}_{ijkl}\gamma_{kl} \quad \forall \gamma_{ij}, \gamma_{kl} \neq 0. \tag{19}$$

Here, the superscripts denote three types of boundary conditions: dd-displacement, dp-displacement periodic, tt-traction. These give

$$C^{(1)(\mathrm{tt})}_{1111} \leqslant C^{(1)(\mathrm{dp})}_{1111} \leqslant C^{(1)(\mathrm{dd})}_{1111} \tag{20a}$$

$$C^{(1)(\mathrm{tt})}_{1212} \leqslant C^{(1)(\mathrm{dp})}_{1212} \leqslant C^{(1)(\mathrm{dd})}_{1212} \tag{20b}$$

$$C^{(1)(\mathrm{tt})}_{1111} - C^{(1)(\mathrm{tt})}_{1212} \leqslant C^{(1)(\mathrm{dp})}_{1111} - C^{(1)(\mathrm{dp})}_{1212} \leqslant C^{(1)(\mathrm{dd})}_{1111} - C^{(1)(\mathrm{dd})}_{1212}. \tag{20c}$$

The last of these results is obtained under $\gamma_{11} = \gamma_{22}$, which makes it a most stringent condition; also, this presupposes the isotropy.

Next, we can adapt the same methodology as that leading to Eq. (19) to prove that the response tensors linking the curvature tensor with the couple–stress tensor follow the fully analogous order relations

$$\kappa_{i3}C^{(2)(tt)}_{i3k3}\kappa_{k3} \leqslant \kappa_{i3}C^{(2)(dp)}_{i3k3}\kappa_{k3} \leqslant \kappa_{i3}C^{(2)(dd)}_{i3k3}\kappa_{k3} \quad \forall \kappa_{i3}, \kappa_{k3} \neq 0, \tag{21}$$

which implies

$$C^{(2)(\mathrm{tt})}_{i3k3} \leqslant C^{(2)(\mathrm{dp})}_{i3k3} \leqslant C^{(2)(\mathrm{dd})}_{i3k3}. \tag{22}$$

All these inequalities are satisfied; Eqs. (20a), (20b) and (22) are given in Table 1, while Eq. (20c) can easily be obtained from these data.

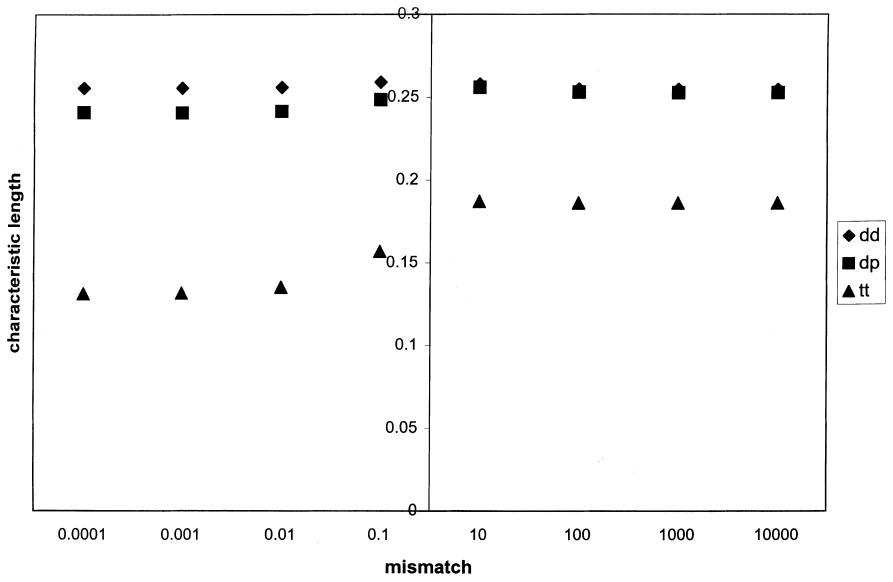

Fig. 8. The characteristic length l, non-dimensionalized by the unit cell size L, as a function of the stiffness ratio $E^{\mathrm{i}}/E^{\mathrm{m}}$ (mismatch), computed from the results of Figs. 5–7. Cases of three boundary conditions are shown.

It is interesting to note that we also find, by our computational mechanics study, the characteristic length l to exhibit this hierarchy (Fig. 8)

$$l^{(\mathrm{tt})} \leqslant l^{(\mathrm{dp})} \leqslant l^{(\mathrm{dd})}. \tag{23}$$

However, we do not have a mathematical proof of Eq. (23). The three plots in Fig. 8 show the characteristic lengths l, resulting from our three types of boundary conditions tt, dp, and dd – all non-dimensionalized by the window size L (=10 in our numerical study). While the right limit of $E^{\mathrm{i}}/E^{\mathrm{m}}$ approximates the situation of rigid grains in the elastic matrix, the left limit approaches that of holes in the elastic matrix (porous material).

With respect to the latter case, we recall that the analytical, micropolar model of triangular beam networks (Woźniak, 1970) gives

$$l^{\mathrm{analytical}} = \frac{L}{24}\,\frac{1+3\left(\frac{w}{L}\right)^2}{1+\left(\frac{w}{L}\right)}. \tag{24}$$

This yields $\cong 0.21$ for beams of the width-to-length (w/L) ratio 1:4 or lower (i.e., from stubby to very slender). The optional correction owing to the Timoshenko, rather than Euler–Bernoulli, beam formulation is negligible. According to Fig. 8, the value 0.21 is clearly bounded (!), respectively, from above and below, by the results of tests conducted under displacement and traction boundary conditions, i.e.

$$l^{(\mathrm{tt})} \leqslant l^{\mathrm{analytical}} \leqslant l^{(\mathrm{dd})}. \tag{25}$$

Inequality (25) shows that the l's we obtained from traction and displacement boundary conditions of the couple–stress theory bound $l^{\mathrm{analytical}}$ resulting from the more correct (and better posed) micropolar theory (Eringen, 1999). Moreover, we note that the displacement-periodic boundary conditions do consistently give $l^{\mathrm{analytical}} < l^{(\mathrm{dp})} < l^{(\mathrm{dd})}$ for the entire range of $E^{\mathrm{i}}/E^{\mathrm{m}}$.

It is important to note two more things here:

(a) The characteristic length l is on the same order for the entire range of E^i/E^m; in Ostoja-Starzewski et al. (1999), it was also found to be the case for three different volume fractions; it changes most dramatically for E^i/E^m ranging from 10^{-2} to 10^2.

(b) As already mentioned earlier in this paper, the particular case of E^i/E^m being exactly unity corresponds to a physically singular situation of a homogeneous medium of the Cauchy type – the same as that of which both classical elastic phases are being made – for which no Cosserat approximation is necessary.

Table 1
$C^{(1)}_{1111}$ (or $C^{(1)}_{2222}$), $C^{(1)}_{1212}$, and $C^{(2)}_{1313}$, non-dimensionalized by E^m, and the corresponding characteristic lengths l, non-dimensionalized by L, obtained by four different boundary conditions: displacement (dd), displacement-periodic (dp), periodic (pp), and traction (tt) for E^i/E^m ranging from 10^{-4} to 10^4 and $v = 0.3$ for volume fraction 18.4% (isotropic cell 10*8.66 ($E^m = 1$))[a]

	dd	dp	tt	pp
$C^{(1)}_{1111}$ or $C^{(1)}_{2222}$				
$E^i/E^m = 0.0001$	0.7284	0.6641	0.0008	0.6627
$E^i/E^m = 0.001$	0.7291	0.6650	0.0083	0.6636
$E^i/E^m = 0.01$	0.7359	0.6734	0.0774	0.6721
$E^i/E^m = 0.1$	0.7968	0.7483	0.4747	0.7474
$E^i/E^m = 10$	1.442	1.440	1.386	1.409
$E^i/E^m = 100$	1.513	1.510	1.428	1.467
$E^i/E^m = 1000$	1.521	1.517	1.436	1.473
$E^i/E^m = 10000$	1.521	1.518	1.436	1.474
$C^{(1)}_{1212}$				
$E^i/E^m = 0.0001$	0.2722	0.2534	0.0004	0.2273
$E^i/E^m = 0.001$	0.2724	0.2537	0.0035	0.2276
$E^i/E^m = 0.01$	0.2744	0.2560	0.0320	0.2306
$E^i/E^m = 0.1$	0.2914	0.2773	0.1767	0.2586
$E^i/E^m = 10$	0.5062	0.4924	0.4733	0.4911
$E^i/E^m = 100$	0.5316	0.5121	0.4864	0.5107
$E^i/E^m = 1000$	0.5345	0.5142	0.4877	0.5128
$E^i/E^m = 10000$	0.5348	0.5145	0.4878	0.5129
$C^{(2)}_{1313}$				dp
$E^i/E^m = 0.0001$	7.118	5.886	0.0024	5.886
$E^i/E^m = 0.001$	7.124	5.897	0.0244	5.897
$E^i/E^m = 0.01$	7.190	5.994	0.2341	5.994
$E^i/E^m = 0.1$	7.820	6.866	1.743	6.866
$E^i/E^m = 10$	13.47	13.32	6.653	13.32
$E^i/E^m = 100$	13.82	13.71	6.771	13.71
$E^i/E^m = 1000$	13.87	13.76	6.786	13.76
$E^i/E^m = 10000$	13.87	13.76	6.786	13.76
Characteristic length				
				pp and dp
$E^i/E^m = 0.0001$	0.2557	0.2410	0.1314	0.2544
$E^i/E^m = 0.001$	0.2557	0.2407	0.1318	0.2545
$E^i/E^m = 0.01$	0.2560	0.2415	0.1352	0.2549
$E^i/E^m = 0.1$	0.2590	0.2486	0.1570	0.2576
$E^i/E^m = 10$	0.2579	0.2559	0.1875	0.2604
$E^i/E^m = 100$	0.2550	0.2531	0.1866	0.2591
$E^i/E^m = 1000$	0.2547	0.2527	0.1865	0.2590
$E^i/E^m = 10000$	0.2547	0.2527	0.1865	0.2590

[a] The columns dd and dp give $C^{(1)}_{2222}$, while tt gives $C^{(1)}_{1111}$ obtained by inversion of the $S^{(1)}_{ijkl}$ tensor.

Finally, the calculated data for the three stiffness constants $C^{(1)}_{1111}$ (or $C^{(1)}_{2222}$), $C^{(1)}_{1212}$, and $C^{(2)}_{1313}$, and the corresponding characteristic lengths l are also given in Table 1. Here, we include the results calculated by displacement (dd), displacement-periodic (dp) and traction (tt) boundary conditions, obtained in this paper and shown in Figs. 5–8, and include for comparison, in the last column, those for $C^{(1)}_{1111}$ and $C^{(1)}_{1212}$ calculated from periodic boundary conditions (pp), reported in Ostoja-Starzewski et al. (1999). Note that the stiffnesses obtained by periodic boundary conditions are also bounded by those calculated by using displacement and traction boundary conditions. The data given in the last column corrects an error which we found in our earlier paper (Ostoja-Starzewski et al., 1999). Namely, a factor $1/2$ was accidentally omitted there in the energy expression in calculation of $C^{(2)}_{1313}$; this resulted in a reported characteristic length smaller by a factor of $\sqrt{2}$. Note that the characteristic length obtained by using periodic/displacement-periodic (pp and dp) boundary conditions is not bounded anymore by the displacement boundary conditions.

Acknowledgements

Support by the NSF under grants CMS-9713764 and CMS-9753075 is gratefully acknowledged.

References

ABAQUS Version 5.6, Hibbit, Karlsson & Sorensen, USA.

Askar, A., 1986. Lattice Dynamical Foundations of Continuum Theories. World Scientific, Singapore.

Bazant, Z.P., Christensen, M., 1972. Analogy between micropolar continuum and grid frameworks under initial stress. Int. J. Solids Struct. 8, 327–346.

Cosserat, E., Cosserat, F., 1909. Théorie des Corps Déformables. A. Herman et Fils, Paris.

Eringen, A.C., 1999. Microcontinuum Field Theories I. Foundations and Solids. Springer, Berlin.

Forest, S., Sab, K., 1998. Cosserat overall modeling of heterogeneous materials. Mech. Res. Comm. 25 (4), 449–454.

Hazanov, S., Huet, C., 1994. Order relationships for boundary conditions effect in the heterogeneous bodies smaller than the representative volume. J. Mech. Phys. Solids 42, 1995–2011.

Herrmann, G., Achenbach, J.D., 1968. Applications of theories of generalized Cosserat continua to the dynamics of composite materials. In: Kröner, E. (Ed.), Mechanics of Generalized Continua, Proc. IUTAM Symposium, 69–79, Springer, Berlin.

Jiang, M., Alzebdeh, K., Jasiuk, I., Ostoja-Starzewski, M., 2000. Scale and boundary conditions effects in elasticity of random composites. Acta Mechanica, in press.

Lakes, R.S., 1983. Size effects and micromechanics of a porous solid. J. Mat. Sci. 18, 2572–2580.

Lakes, R.S., 1986. Experimental microelasticity of two porous solids. Int. J. Solids Struct. 22, 55–63.

Lakes, R., 1995. Experimental methods for study of Cosserat elastic solids and other generalized elastic continua. In: Mühlhaus, H.-B. (Eds.), Continuum Models for Materials with Microstructure. John Wiley, Chichester, pp. 1–25.

Nowacki, W., 1986a. Theory of Asymmetric Elasticity. Oxford, Pergamon Press.

Nowacki, W., 1986b. Advances in Theory of Elasticity. Polish Scientific Publishers, Warsaw, in Polish.

Ostoja-Starzewski, M., Boccara, S., Jasiuk, I., 1999. Couple-stress moduli and characteristic length of composite materials. Mech. Res. Comm. 26 (4), 387–397.

Ostoja-Starzewski, M., Jasiuk, I., 1995. Stress invariance in planar Cosserat elasticity. Proc. Roy. Soc. Lond. A 451, 453–470.

Perkins, R.W., Thomson, D., 1973. Experimental evidence of a couple-stress effect. AIAA J. 11, 1053–1055.

Sanchez-Palencia, E., Zaoui, A. (Eds.), 1987. Homogenization Techniques for Composite Media. Lecture Notes in Physics 272.

Woźniak, C., 1970. Surface Lattice Structures. Polish Scientific Publishers, Warsaw, in Polish.

Yang, J.F.C., Lakes, R.S., 1982. Experimental study of micropolar and couple-stress elasticity in bone in bending. J. Biomech. 15, 91–98.